Finite element analysis of single-edge-cracked rolled high-density polyethylene

Min-Diaw Wang*, Eiji Nakanishi† and Sadao Hibi
Department of Materials Science and Engineering, Nagoya Institute of Technology, Gokiso-Cho, Showa-Ku, 466 Nagoya, Japan
(Received 1 February 1993; revised 11 May 1993)

Stress and strain distributions around the crack tip of rolled high-density polyethylene have been analysed using the two-dimensional finite element method. Mechanical parameters from two samples were used. The highly anisotropic sample showed distinct differences in Young's moduli and yield stresses *versus* various off-axis angles while the sample of low anisotropy showed high moduli and yield stresses in both the roll and the transverse direction. Calculated results revealed a strong relation between the stress distributions at the crack front and the anisotropy of the materials. The sample with high anisotropy showed intense stress distributions coincident with the chain axis. In contrast, stress distributions of the sample with low mechanical anisotropy were less affected by the alignment of the chain axis. From experiment, kinky deformation was observed for some cases. Comparison of the experimental with the calculated results threw light on the mechanism of formation of a kink band during restretching of anisotropic polymers.

(Keywords: finite element analysis; rolled high-density polyethylene; anisotropy)

INTRODUCTION

The study of the anisotropic behaviour of oriented polymers can be traced back for several decades. During the 1960s, researchers noticed that oriented polymers showed slip bands and kink bands, as seen in metals in the form of slippage along the crystallographic planes. Observation of the deformation and interpretation of the behaviour have been extensively studied in the intervening years. Different conclusions have been reached. The deformation band is thought by some workers to be due to slippage of the chain, while others argue that it originates from kinking of molecular chains. Young *et al.*[1] measured compression on oriented HDPE and concluded that the principal mechanism of plastic deformation was by [0 0 1] crystallographic slip along the chain direction. From shear experiments on oriented polycarbonate and polyphenylene oxide[2], and HDPE and PP[3,4], Robertson came to the conclusion that the yield process was associated with the kinking of the chains due to shearing. Tajima[5] concluded from compression studies on thick oriented HDPE that kink bands did not occur because of chain slippage but due to interlamellar shear of the lamellar block. Ward and co-workers[6–8] have made a major contribution to the study of oriented crystalline polymers. Ward interpreted plastic deformation in a quite different manner from other researchers. Defining the angle between the test direction and the chain direction as the off-axis angle β, Ward argued that plastic deformation originated from shearing which was different in resulting direction from that proposed by Robertson, and was able to interpret why the band direction was different from the chain direction. Macroscopic mechanical behaviour was studied by Rider and Hargreaves[9]. While the above contributors investigated uncracked samples only, Parrish and Brown[10] notched oriented poly(ethylene terephthalate) and found that the deformation band originated from the notched position. The deformation bands obtained in this way were basically the same as those without a notch. Existence of a notch provided the origin of global plastic deformation such as slippy or kinky deformation. However, no stress analysis on oriented polymers is reported in the work described above. The plastic deformation that originates from the crack tip during off-axis angle testing is believed to be either the slip band, the kink band or both, depending on the relation between the stretch direction and the chain axis direction. Stress analysis of the deformation at the crack tip will therefore be a powerful approach in elucidating the mechanism of plastic deformation in oriented polymers.

Fracture mechanism and energy analysis of rolled high-density polyethylene (HDPE) along the roll direction (RD, chain axis) have been studied in previous papers[11,12]. The effect of molecular weight on the anisotropic behaviour has been discussed. Fracture energy in the chain axis was evaluated and its relation to the molecular weight was established. It was concluded that the tie chains and entanglements among the crystalline blocks were responsible for the difference in the texture, anisotropic mechanical behaviour and fracture mechanism. However, fracture tests in directions with off-axis angles other than 90° resulted in complicated plastic deformation and the fracture energy was not able to be evaluated. An off-axis angle of 90° means stretching the specimen in a direction perpendicular to the chain

* Present address: Analytical Research Department, Central Research Institute, Mitsui Toatsu Chemicals, Inc., Japan
† To whom correspondence should be addressed

0032-3861/94/07/1442–10

axis (the transverse direction). Analysis of the stress distribution at the crack tip should be helpful in understanding the fracture mechanism. The finite element method (FEM) is used to handle this task. The material will be treated as a continuum and only the global mechanical parameters, instead of molecular weight or structure, are to be used for calculation.

FINITE ELEMENT METHOD

For clarity, the FEM simulation will be introduced in four stages. First, the construction of the elements is presented. Second, since the material is anisotropic, the von Mises yield criterion can no longer be used. The theory of plasticity is therefore introduced. Third, since fracture of the specimen is studied at various off-axis angles, it is necessary to introduce the transformation of coordinates. The stiffness matrix and strength tensor are therefore related to material constants measured from experiments. Finally, the mechanical behaviour after yielding is derived by modifying the stiffness matrix into the plastic matrix.

Establishment of the elements

The layout of the elements is shown in *Figure 1*, and the relation of the orientation with the coordinates is shown in *Figure 2*. The β value is defined as the off-axis angle and θ is the angle between any vector and the crack plane. For convenience, stress distribution around the crack tip will be presented as a function of θ.

Theory of plasticity for anisotropic materials

According to Tsai and Wu[13], the strength potential of a material can be defined as:

$$f^2(\sigma_k)=F_i\sigma_i^2+F_{ij}\sigma_i\sigma_j=\sigma_e^2 \quad (1)$$

where σ_e is the equivalent stress and F_i and F_{ij} are components of the strength tensor. The material yields when the equivalent stress equals the yield stress, that is:

$$f^2(\sigma_k)=\sigma_Y^2 \quad (2)$$

In the case of plane stress and neglecting the hydrostatic effect, the strength potential can be written as:

$$F_{11}\sigma_{x1}^2+F_{22}\sigma_{x2}^2+F_{66}\tau_{x1x2}^2+2F_{12}\sigma_{x1}\sigma_{x2}=\sigma_Y^2 \quad (3)$$

where τ is the shear stress. F_{11}, F_{22} and F_{66} can be determined by stretching the sample with an off-axis angle of 0°, 90° and 45°, respectively. Because the stability conditions must be established, equation (3) must be a function of an ellipse so that the curve is self-closed. Therefore F_{12} has to meet the following requirement:

$$\sqrt{F_{22}-1}<F_{12}<\sqrt{F_{22}} \quad (4)$$

In this work, F_{12} is defined as:

$$F_{12}=\tfrac{1}{2}(\sqrt{F_{22}-1}+\sqrt{F_{22}}) \quad (5)$$

The strength potential is independent of transformation of coordinates while the components have to be transformed during off-axis angle stretching.

Coordinate transformation

Compliance matrix. For an O–$X_1X_2X_3$ Cartesian coordinate, the strain, S, and stress, σ, can be related as follows:

$$[\varepsilon_{ij}]=[S_{ijkl}][\sigma_{kl}] \quad (6)$$

As shown in *Figure 3*, a rectangular specimen is cut out of the anisotropic material. Let the new coordinate used to define the specimen be defined as O–$X'_1X'_2X'_3$. Relation

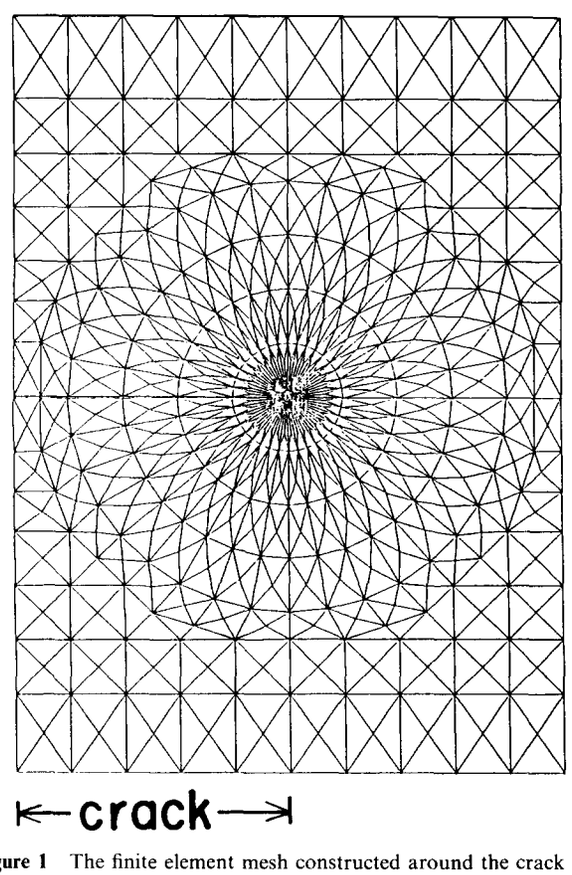

Figure 1 The finite element mesh constructed around the crack tip

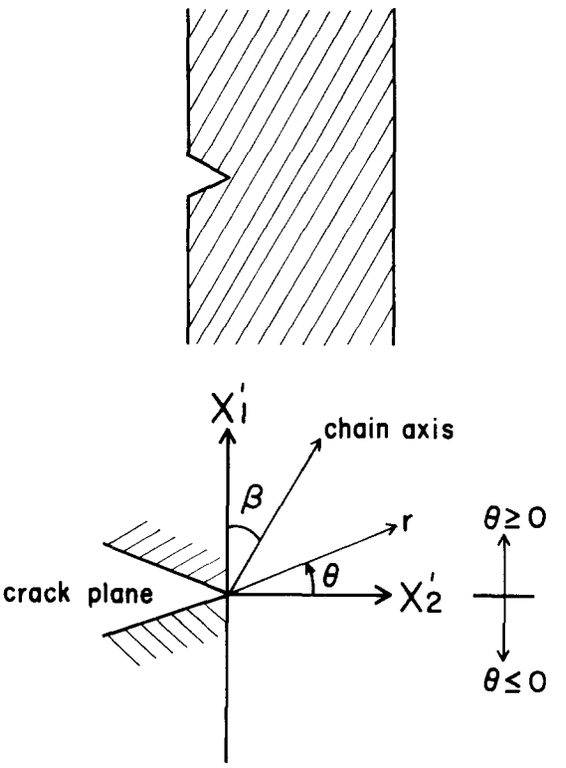

Figure 2 Relation of the chain axis to the coordinates (viewed from the X'_3 axis)

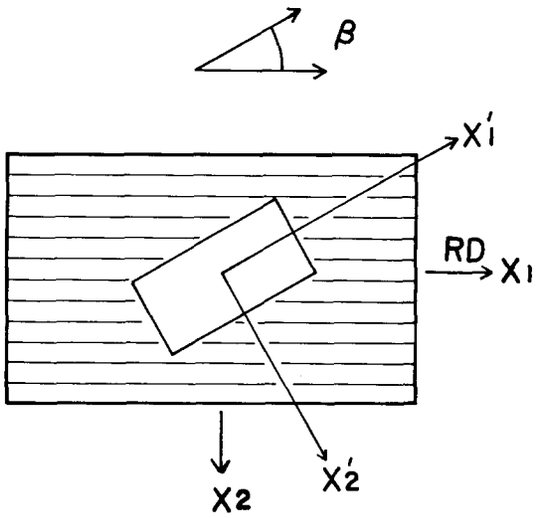

Figure 3 Relation of the specimen coordinates to the roll direction (RD). Off-axis angle β implies the angle between the roll direction and the restretch direction (viewed from the X'_3 axis)

of these two coordinates can be expressed as:

$$\begin{bmatrix} X'_1 \\ X'_2 \\ X'_3 \end{bmatrix} = \begin{Bmatrix} \cos\beta & -\sin\beta & 0 \\ \sin\beta & \cos\beta & 0 \\ 0 & 0 & 1 \end{Bmatrix} \begin{bmatrix} X_1 \\ X_2 \\ X_3 \end{bmatrix} \quad \text{or} \quad X'_m = a_{mi} X_i \tag{7}$$

In the O–$X'_1X'_2X'_3$ coordinate, the relation between strain and stress is:

$$[\varepsilon'_{mn}] = [S'_{mnop}][\sigma'_{op}] \tag{8}$$

With the help of equation (7), S'_{mnop} can be related to S_{ijkl} as:

$$S'_{mnop} = a_{mi}a_{nj}a_{ok}a_{pl}S_{ijkl} \tag{9}$$

where a_{mi} relates X_i to X'_m. The stiffness matrix is just the inverse of the compliance matrix.

Strength tensor. Without considering the hydrostatic effect, equation (1) can be rewritten as follows with some rearrangement of the index notation:

$$f^2(\sigma_k) = F_{ijkl}\sigma_{ij}\sigma_{kl} = \sigma_e^2 \tag{10}$$

Because the potential is independent of coordinate, in the O–$X'_1X'_2X'_3$ coordinate, the potential is

$$f^2(\sigma_k) = F'_{mnop}\sigma'_{mn}\sigma'_{op} = \sigma_e^2 \tag{11}$$

F'_{mnop} can be derived by replacing σ'_{mn} with σ_{ij} using the following relation:

$$\sigma'_{kl} = a_{ki}a_{lj}\sigma_{ij} \tag{12}$$

The relation between F'_{mnop} and F_{ijkl} can be established by comparing the coefficients of σ_{ij}. In fact, the transformation of the compliance matrix and of the strength tensor are exactly the same.

Construction of the plastic constitutive equation

In the case of an elastic solid, the relation between the strain and stress is as follows:

$$[\varepsilon] = [S^e][\sigma] \quad \text{or} \quad [\sigma] = [C^e][\varepsilon] \tag{13}$$

where $[C^e] = [S^e]^{-1}$. After the material yields, the incremental strain can be expressed as:

$$\{d\varepsilon\} = \{d\varepsilon^e\} + \{d\varepsilon^p\}$$

or

$$\{d\varepsilon^e\} = \{d\varepsilon\} - \{d\varepsilon^p\} \tag{14}$$

where $d\varepsilon^e$ and $d\varepsilon^p$ are the elastic incremental strain and the plastic incremental strain, respectively. Substituting equation (13) into equation (14), one obtains:

$$\{d\sigma\} = [C^e]\{d\varepsilon\} - [C^e]\{d\varepsilon^p\} \tag{15}$$

As mentioned above, the strength potential may be defined as the plastic potential even after yielding. Then, by referring to *Figure 4*, $\{d\varepsilon^p\}$ can be defined as

$$\{d\varepsilon^p\} = h \cdot \left\{\frac{\partial f}{\partial \sigma}\right\} df \tag{16}$$

where h is a constant which can be derived as follows.

After yielding, the plastic strain energy is defined as:

$$dw^p = \{\sigma\}^T\{d\varepsilon^p\} = \bar{\sigma} \cdot d\bar{\varepsilon}^p \tag{17}$$

where σ and $d\varepsilon^p$ are the equivalent stress and incremental strain. Substituting equation (16) into (17), one obtains:

$$h\, df = \frac{\bar{\sigma}}{\{\sigma\}^T\{\partial f/\partial\sigma\}} d\bar{\varepsilon}^p \tag{18}$$

Usually, the material undergoes strain hardening after yielding. From experiment, the strain hardening factor, H, can be measured and is defined as:

$$\frac{d\bar{\sigma}}{d\bar{\varepsilon}^p} = H \tag{19}$$

Substituting equation (19) into (18), one obtains

$$h\, df = \frac{\bar{\sigma}}{\{\sigma\}^T\{\partial f/\partial\sigma\}} \cdot \frac{d\bar{\sigma}}{H} \tag{20}$$

From equation (11):

$$\left\{\frac{df}{\partial\sigma}\right\} = \frac{1}{f}\begin{bmatrix} F'_{11}\sigma'_{x1} + F'_{12}\sigma'_{x2} + F'_{16}\tau'_{x1x2} \\ F'_{22}\sigma'_{x2} + F'_{12}\sigma'_{x1} + F'_{26}\tau'_{x1x2} \\ F'_{66}\tau'_{x1x2} + F'_{16}\sigma'_{x1} + F'_{26}\sigma'_{x2} \end{bmatrix} \tag{21}$$

Consequently

$$\{\sigma\}^T\left\{\frac{\partial f}{\partial\sigma}\right\} = \frac{1}{f}(F'_{11}\sigma'^2_{x1} + F'_{22}\sigma'^2_{x2} + F'_{66}\tau'^2_{x1x2} + 2F'_{12}\sigma'_{x1}\sigma'_{x2} + 2F'_{16}\sigma'_{x1}\tau'_{x1x2} + 2F'_{26}\sigma'_{x2}\tau'_{x1x2} = \frac{1}{f}f^2 = f = \bar{\sigma} \tag{22}$$

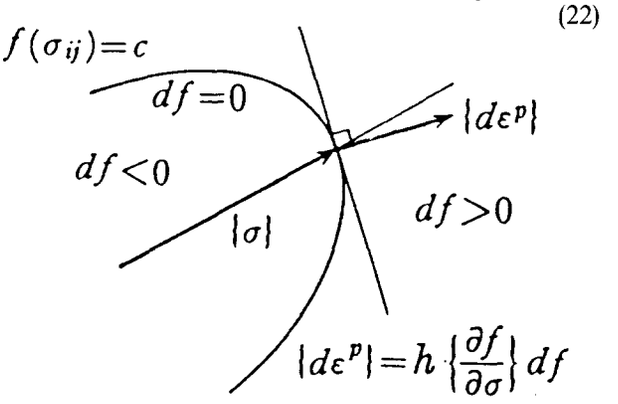

Figure 4 Schematic representation of the yield surface and the path of the strength potential after yielding

Substituting equation (22) into (21), one obtains

$$h \cdot df = \frac{\bar{\sigma}}{\bar{\sigma}} \cdot \frac{d\bar{\sigma}}{H} = \frac{df}{H} \Rightarrow h = \frac{1}{H} \tag{23}$$

After h is derived, derivation of the plastic constitutive equation can be continued. Equation (15) now becomes

$$\{d\sigma\} = [C^e]\{d\varepsilon\} - [C^e] \cdot h \cdot \left\{\frac{df}{\partial\sigma}\right\} df \tag{24}$$

and

$$df = \frac{\partial f}{\partial \sigma'_{x1}} d\sigma'_{x1} + \frac{\partial f}{\partial \sigma'_{x2}} d\sigma'_{x2} + \frac{\partial f}{\partial \tau'_{x1x2}} d\tau'_{x1x2}$$

$$= \frac{\partial f}{\{\partial\sigma\}^T} \{d\sigma\} \tag{25}$$

Substituting equation (25) into (24), one obtains:

$$df = \frac{\partial f}{\{\partial\sigma\}^T} [C^e]\{d\varepsilon\} - \frac{1}{H} \frac{\partial f}{\{\partial\sigma\}^T} [C^e] \left\{\frac{\partial f}{\partial\sigma}\right\} df \tag{26}$$

$h\,df$ can be derived as:

$$h\,df = \frac{1}{H} df = \frac{\{\partial f/\partial\sigma\}^T [C^e]\{d\varepsilon\}}{H + \{\partial f/\partial\sigma\}^T [C^e]\{\partial f/\partial\sigma\}} \tag{27}$$

so that, after yielding, the relation between $\{d\sigma\}$ and $\{d\varepsilon\}$ can be dexpressed as:

$$\{d\sigma\} = \left\{[C^e] - \frac{[C^e]\{\partial f/\partial\sigma\}\{\partial f/\partial\sigma\}^T[C^e]}{H + \{\partial f/\partial\sigma\}^T[C^e]\{\partial f/\partial\sigma\}}\right\}\{d\varepsilon\} \tag{28}$$

$$= [C^p]\{d\varepsilon\} \tag{29}$$

Here $[C^p]$ is defined as the plastic stiffness matrix for material after yielding.

Determination of yielding by calculation

Yielding of the elements is checked if the equivalent stress of any element calculated by the strength tensor equals the yield stress. In order to confirm that yielding proceeds stepwisely, the R_{min} method[14] is used. Since it was originally designed for isotropic solids, application of the R_{min} method to anisotropic solids is only good for approximation during small deformation because extension of the yield surface of anisotropic solids should be quite different from that of isotropic solids.

EXPERIMENTAL

Two samples were used. Sample A had a weight-average molecular weight of 17×10^4 and birefringence of 0.051. The molecular weight of sample B was 98×10^4 and the birefringence was 0.041. Fundamental data of these two samples are summarized in *Table 1*. For both uncracked and cracked specimens, the dimensions were 60 mm in gauge length and 20 mm in width. For cracked specimens, samples were single-edge cracked with a sharp razor-blade and the initial crack lengths were all 10 mm. The specimens were stretched at a speed of 5% min^{-1}. Initial modulus was taken as the slope at a strain of $< 1\%$. The yield stress of an uncracked specimen was taken as the intersect of the initial slope and the tangential line at a strain of 3%. Mechanical parameters such as Young's modulus, yield stress, Poisson ratio and strain hardening index were used as input data for calculation. Pictures of the kink band deformation of sample B were taken. Wide-angle X-ray diffraction (WAXD) was applied to study the chain axis orientation inside the kink band.

Table 1 Basic physical properties of samples

Sample	M_w ($\times 10^4$)	Birefringence, Δ	Density, ρ (g cm^{-3})	Processing temperature, T_{proc} (°C)[a]
A	17	0.051	0.964	115
B	98	0.041	0.955	125

[a] Because of the strong retraction of sample B, the processing temperature for this sample has to be higher

RESULTS AND DISCUSSION

The calculation was performed using mechanical parameters from samples A and B as mentioned previously. These two samples were selected because sample A possessed high mechanical anisotropy while sample B exhibited low mechanical anisotropic behaviour. Of course, for FEM calculations the length of the molecular chain (molecular weight) is not taken into account, as only the global mechanical parameters were used. The sample dimensions for calculation were the same as for experiment and the initial crack length was set at 10 mm.

Figure 5 shows the Young's moduli and yield stresses *versus* off-axis angles of samples A and B. It can be seen that both the Young's modulus and yield stress of sample A were higher in the roll direction than in any other off-axis angle. Thus the orientation effect from rolling was distinguished. On the other hand, sample B showed high Young's modulus and yield stress in the transverse direction. As discussed in previous papers[11,12], this may be due to the existence of more tie chains and entanglements among crystalline blocks for the high-molecular-weight sample. Consequently, the orientation effect from rolling of sample B was not as pronounced as that of sample A. The Young's moduli of cracked samples are presented in *Figure 6*. Good agreement was confirmed between calculation and experiments. Basically, the cracked and uncracked samples showed a similar relationship between Young's moduli and off-axis angles. Cracking resulted in reducing the Young's moduli in value but not the anisotropy.

To understand the effect of the dimension and mode of fracture, a calculation was performed with mechanical parameters of an arbitrarily assumed isotropic material with Young's modulus of 4.9 GPa and yield stress of 62 MPa. The stress distribution *versus* θ of an isotropic material is presented in *Figure 7*. σ_{xx} represents the stress in the stretch direction, τ_{xy} is the shear stress and σ_e is the equivalent stress (the stress potential). In this calculation, it was found that the stress distributions were similar for positions with different distances from the crack tip. The only difference was the magnitude. The stress distributions for isotropic and anisotropic materials will thus be presented with the same r value (the distance from the crack tip) of 3 mm. The stress distributions in *Figure 7* were similar to those derived from the linear elastic fracture mechanism (LEFM) for mode 1 fracture. The stress distribution around the crack tip of an isotropic material is symmetrical in the crack plane. Plus or minus signs of the shear stress imply opposite acting directions. For an isotropic sample, this will not result in either slipping or kinking of the molecular chain. With such

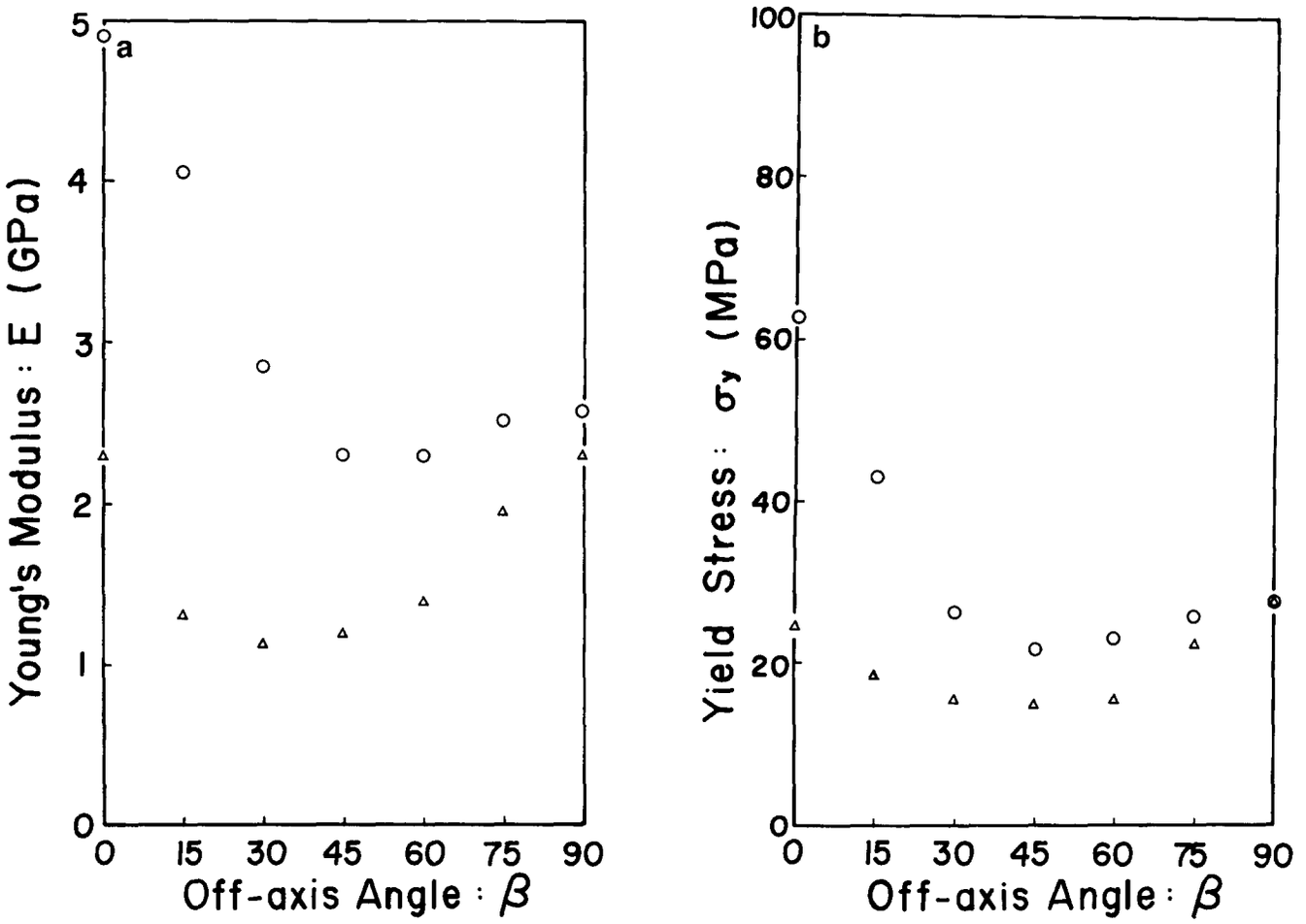

Figure 5 The Young's moduli (a) and yield stresses (b) *versus* off-axis angles of uncracked samples A (○) and B (△)

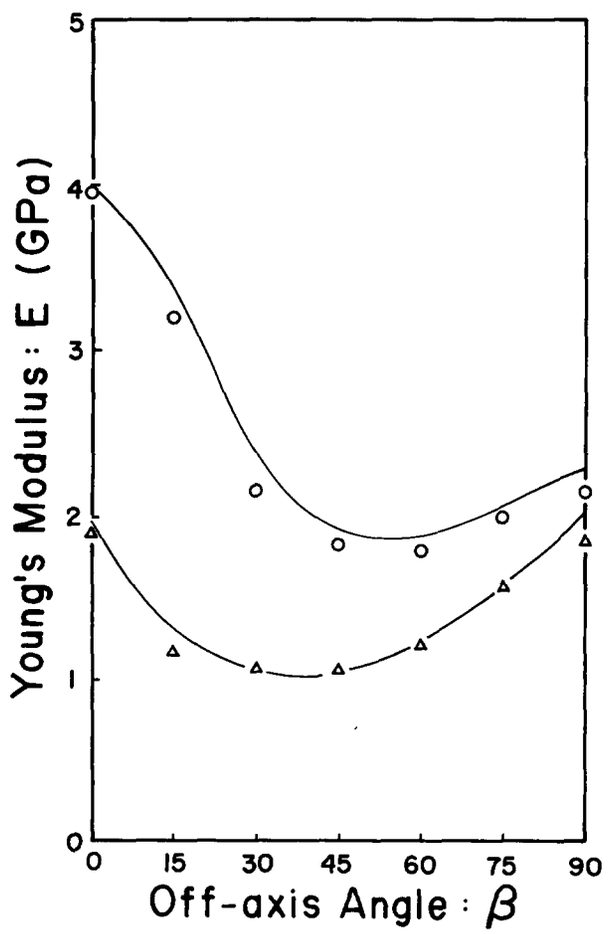

Figure 6 Comparison of the Young's modulus from calculation (curves) and experiment (symbols): (○), cracked sample A; (△), cracked sample B

information from isotropic material in mind and with the help of the anisotropic behaviour shown in *Figure 5*, it is easier for one to visualize the anisotropic effect on cracked samples as more results are presented.

Figure 8 shows the calculation of the distribution of σ_{xx} of sample A with off-axis angles of 15° and 75°. Compared with *Figure 7a*, sample A showed unsymmetrical distribution with respect to the crack plane, especially for an off-axis angle of 15°, where the maximum of the stress distribution was coincident with the alignment of the chain axes. For off-axis angles of 75°, the molecular chains were aligned closer to the crack plane and the σ_{xx} distribution seemed to become more symmetrical with respect to the crack plane. As mentioned previously, the θ value is different from the off-axis angle β. The direction of the chain axis can be expressed in terms of θ with the following relation. Let θ_c be the chain axis direction, then

$$\theta_c = 90 - \beta \tag{30}$$

In *Figure 8b*, the off-axis angle is 75°, that is, the chain axis is aligned at $\theta = 15°$. It can be seen that a maximum appeared at $\theta = -75°$, which corresponded to the transverse direction of the molecular chain. Appearance of this maximum is believed to be partly due to the intrinsic dimension effect of mode I fracture mechanics (e.g. *Figure 7a*) and partly due to the higher strength in

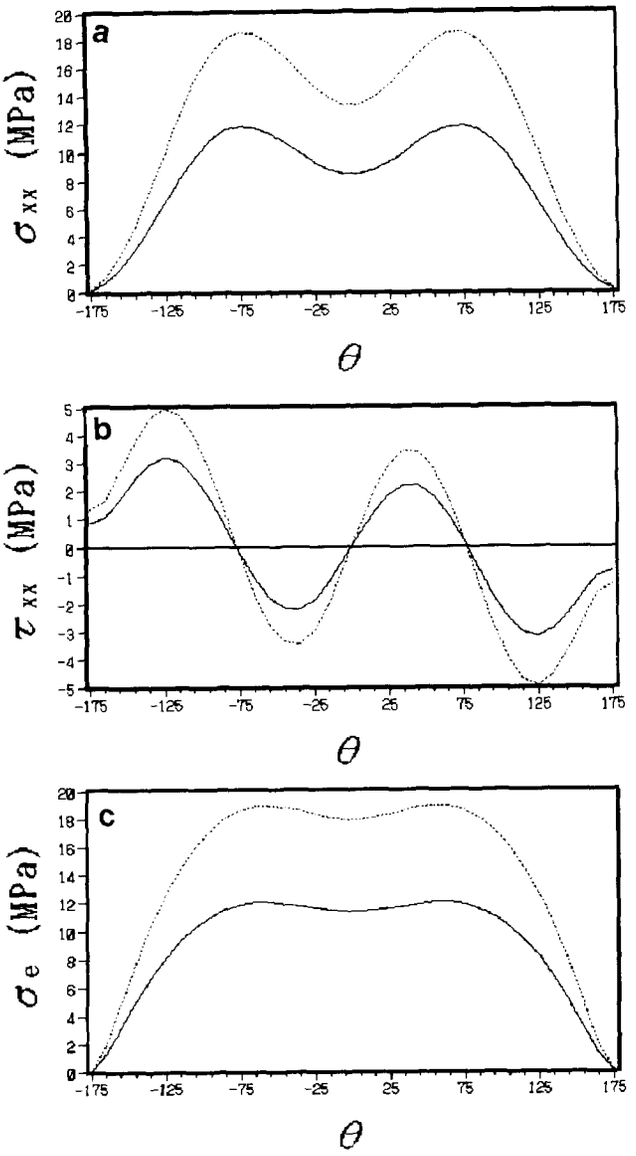

Figure 7 Stress and strain distribution of isotropic material, for $r = 3$ mm. Extent of stretching: ——, 0.25 mm; ···, 0.50 mm. θ is defined in *Figure 2*

the transverse direction of the molecular chain when compared with that of some other off-axis angles (see *Figure 5*). Distribution of σ_{yy} was not affected by the orientation significantly and therefore will not be discussed in detail. Distribution of τ_{xy} did show dependence on the alignment of the chain axis. For isotropic material, τ_{xy} is symmetrical with respect to the crack plane (*Figure 7b*). In *Figure 9*, τ_{xy} above the crack plane ($\theta > 0$) was more intense than below the crack plane ($\theta < 0$) for small off-axis angle values. As the chain axis was aligned closer to the crack plane, τ_{xy} below the crack plane became more predominant. The physical meaning of the sign of τ_{xy} is schematically presented in *Figure 10*. Positive τ_{xy} resulted in shearing of the molecular chain while negative τ_{xy} resulted in kinking of the molecular chain. That is, as the off-axis angle increased, the molecular chain under the crack plane tended to be kinked more intensely. The strength potential (the equivalent stress, σ_e), as derived according to equation (3) for sample A, is shown in *Figure 11*. As sample A was a material showing high anisotropy, the distribution of σ_e was affected by the alignment of the chain axis. For off-axis angles less than 45°, the maximum of the distribution of σ_e was coincident with the chain axis direction. As the molecular chains were aligned toward the crack plane, the stress under the crack plane became more intense. As the molecular chains were aligned

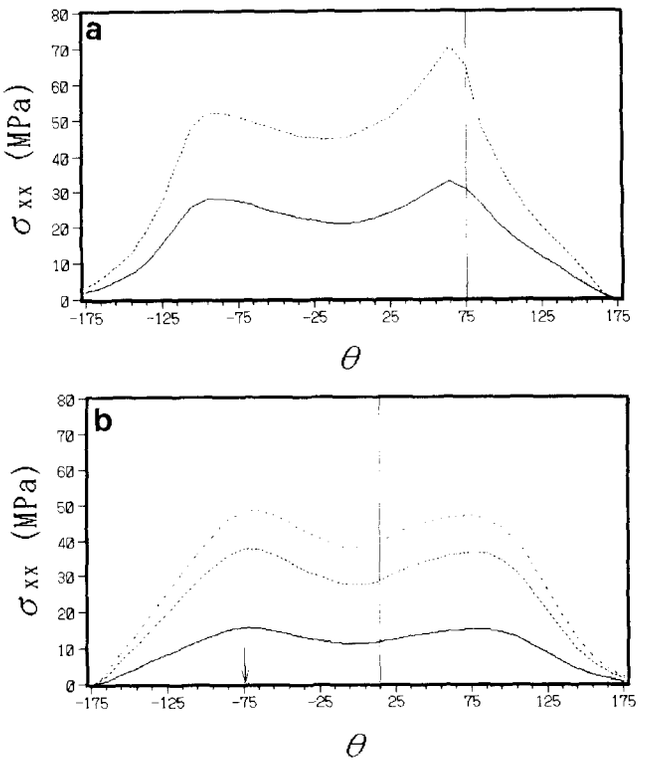

Figure 8 Distribution of σ_{xx} of sample A with off-axis angles (a) 15° and (b) 75°. Extent of stretching: ——, 0.25 mm; ···, 0.5 mm; ·····, 0.75 mm. The vertical solid line indicates the chain axis direction while the arrow (↓) indicates the direction transverse to the chain axis

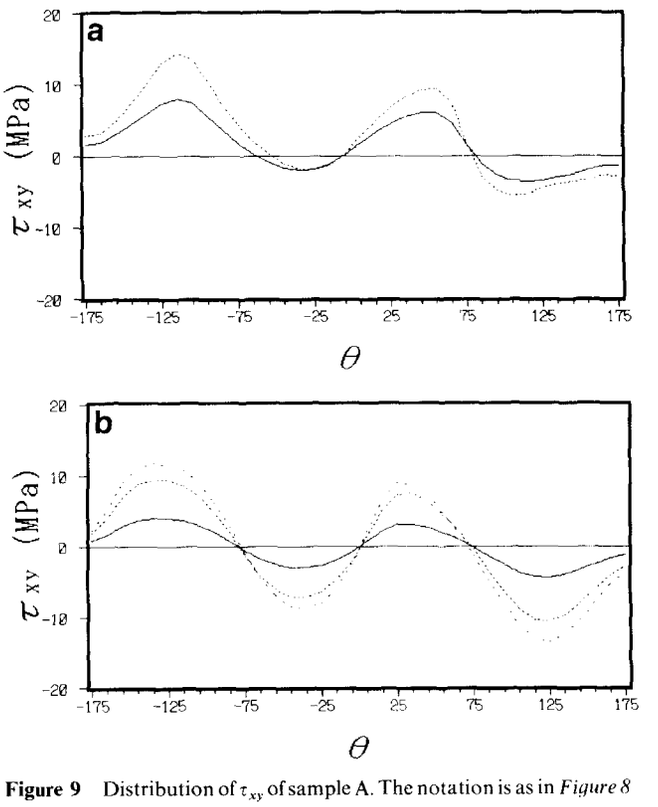

Figure 9 Distribution of τ_{xy} of sample A. The notation is as in *Figure 8*

parallel with the crack plane, the distribution became symmetrical with respect to the crack plane. Even for sample A, which possessed high anisotropy, as the molecular chains were aligned closer to the crack plane, the stress distributions tended to be more dominated by the fracture mode and the mechanical behaviour transverse to the chain axis.

As shown in *Figure 5*, sample B was a material with less anisotropy. Calculation results showed a strong relationship between the distributions of stress with such an intrinsic mechanical property. *Figure 12* shows the distribution of σ_{xx} for sample B. For samples with an off-axis angle $<45°$, a maximum did show up at a value of θ coincident with the chain axis direction but it was not as predominant as that of sample A. As the molecular chains were aligned toward the crack plane, maxima both above and below the crack plane showed up at a value of θ coincident with the direction transverse to the chain axis. This can be explained by referring to *Figure 5*.

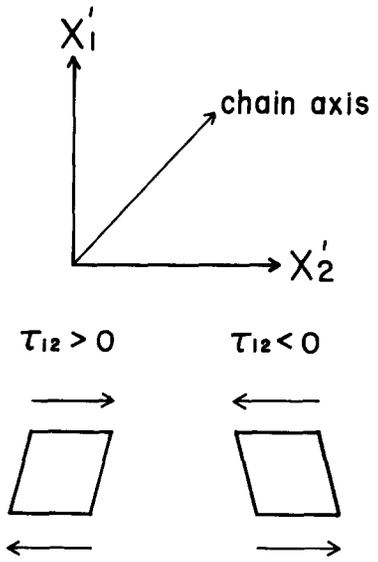

Figure 10 Schematic representation of the physical meaning of τ_{12} (τ_{xy}). Positive τ_{12} results in shearing of the chains while negative τ_{12} results in kinking of the chains

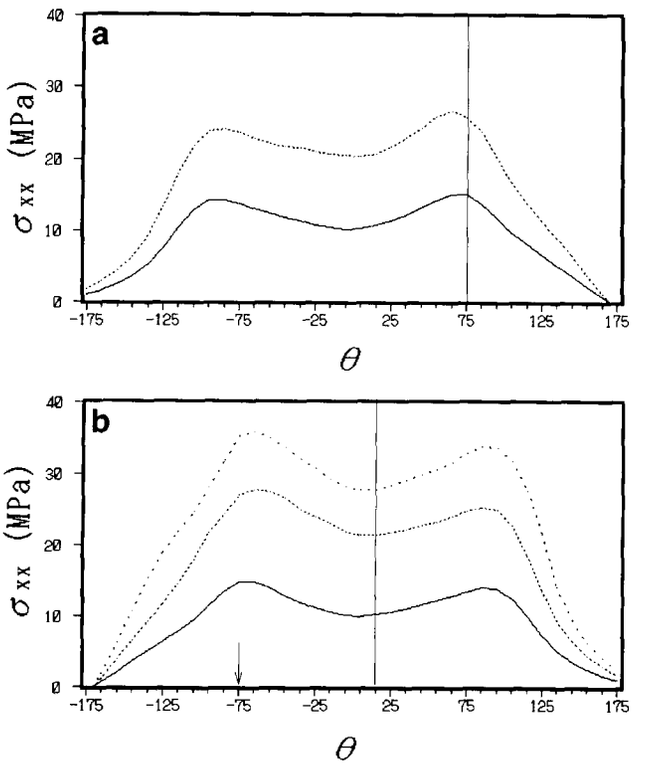

Figure 12 Distribution of σ_{xx} of sample B. The notation is as in *Figure 8*

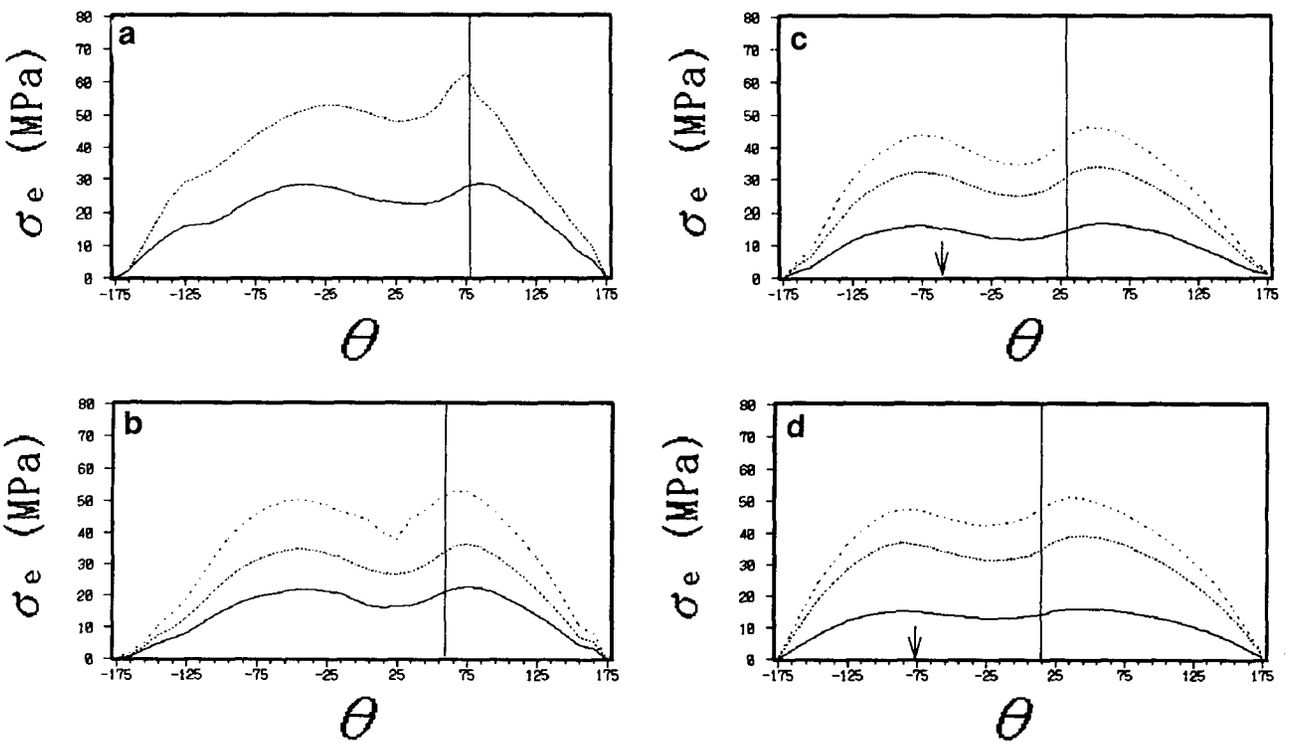

Figure 11 Distribution of σ_e of sample A. The notation is as in *Figure 8* with off-axis angles of (a) 15° (b) 30° (c) 60° and (d) 75°

Sample B showed high modulus in the direction transverse to the chain axis and this, in turn, affected the stress distribution around the crack tip. The distribution of σ_{yy} was also not significantly affected by the alignment of the chain axis. The shear stress distribution of sample B is shown in *Figure 13*. Compared with both the isotropic material and sample A, the τ_{xy} under the crack plane with a negative value was much more intense than that above the crack plane. Such shear stress, as mentioned previously, would result in kinking of the molecular chain. Hibi and co-workers[15] performed FEM analysis on uncracked rolled HDPE and concluded that shear stress, resulting in kinking the molecular chain, was intense for off-axis angles greater than 45°. In this work, the crack provided the location for the origin of stress concentration. Distribution of σ_e of sample B is shown in *Figure 14*. Unlike sample A, which showed clear differences for various off-axis angles, sample B showed little change of the σ_e distribution with off-axis angle. Attention should be paid to cases with off-axis angles greater than 45°. Comparison of *Figure 14* with *Figure 11* shows that sample B showed more intense σ_e distribution under the crack plane than above the crack plane. Therefore, plastic deformation of sample B under the crack plane should be more intense than above the crack plane. With the information from distributions of σ_e and τ_{xy}, it is expected that kinky deformation under the crack plane of sample B would be predominant for off-axis angles larger than 45°.

As was discussed previously[12], sample A was a material fracturing in a brittle manner with a fracture energy along the chain axis of 0.55 kJ m^{-2}. From the above calculation, the stress distribution in the chain axis direction was always the most intense. Consequently, with small fracture energy and stress concentration at the crack tip along the chain axis, sample A is expected to show brittle fracture at any off-axis angle stretching. From experiment, it was found that sample A did show brittle fracture with small deformation for every off-axis angle. It was therefore not possible to investigate slip or kink plastic deformation of sample A. On the other hand, sample B showed ductile fracture with global plastic deformation and the fracture

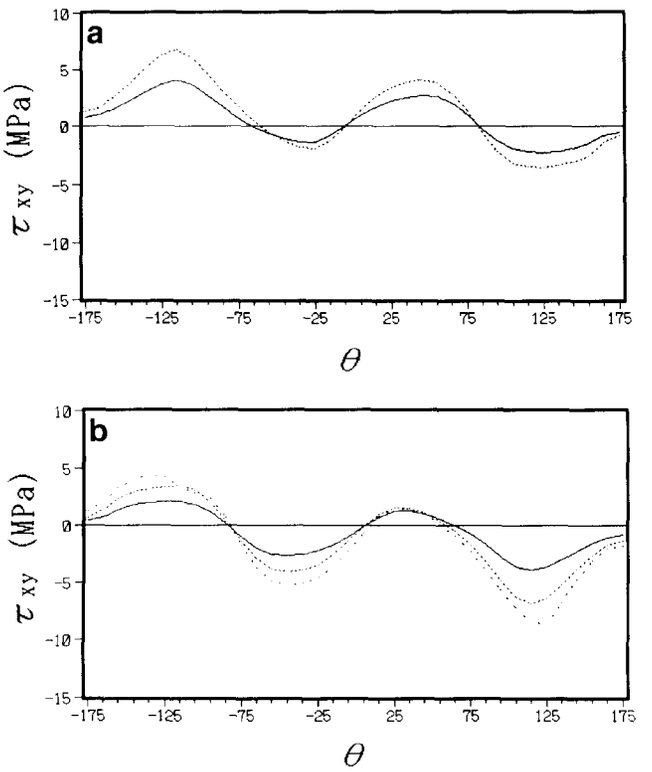

Figure 13 Distribution of τ_{xy} of sample B. The notation is the same as *Figure 8*

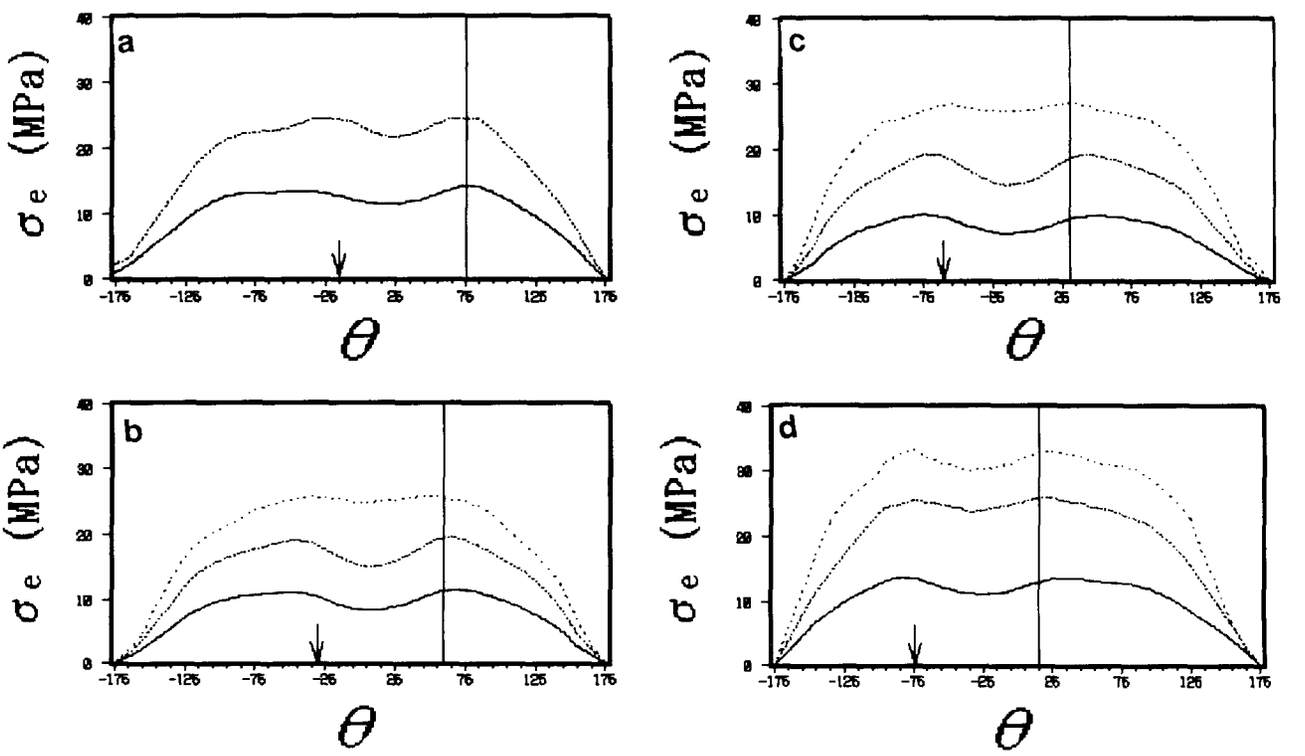

Figure 14 Distribution of σ_e of sample B. The notation is as in *Figure 8* with off-axis angles of (a) 15° (b) 30° (c) 60° and (d) 75°

energy was 4.1 kJ m^{-2} along the chain axis. The FEM calculation showed that, for off-axis angles >45°, stress or strain concentration was not coincident with the chain axis, and shear stress resulting in kinking of the molecular chain was predominant under the crack plane. A plot of the isoequivalent stress of sample B is presented in *Figure 15* for an off-axis angle of 75°. It is clear that the stress distribution under the crack plane is quite intense. Experimental results are presented in *Figure 16* for off-axis angles of 45°, 60° and 75°. These pictures were taken with samples placed between cross-Nicols. The intense deformation above the crack plane was believed to be due to [0 0 1] crystallographic slippage deformation.

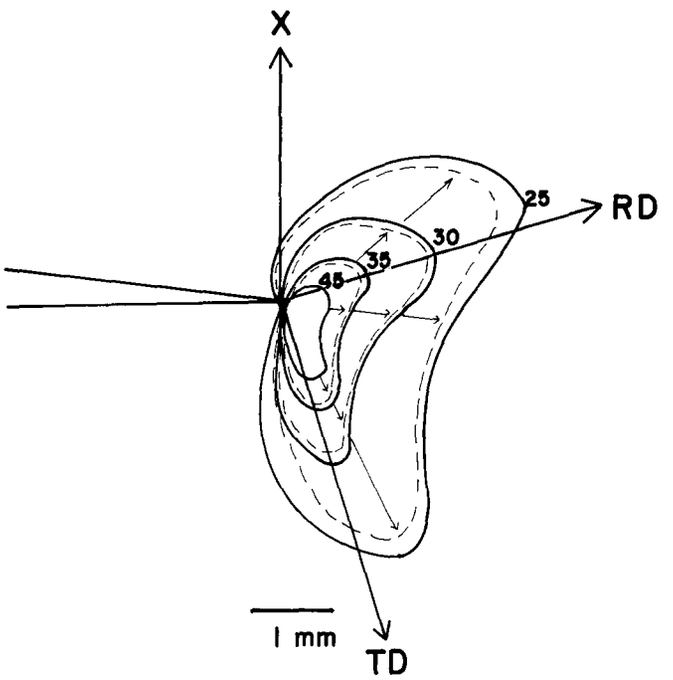

Figure 15 The iso-σ_e distribution at the crack tip of sample B with off-angle of 75°. Numbers on the figure represent the σ_e values

A kink band appeared as the bright part under the crack plane and was a plastically deformed region with molecular chains reoriented from the roll direction. Calculation from FEM was quite consistent with the experimental results. To investigate the orientation of molecular chains inside the kink band, wide-angle X-ray diffraction patterns are shown in *Figure 17*. Before testing,

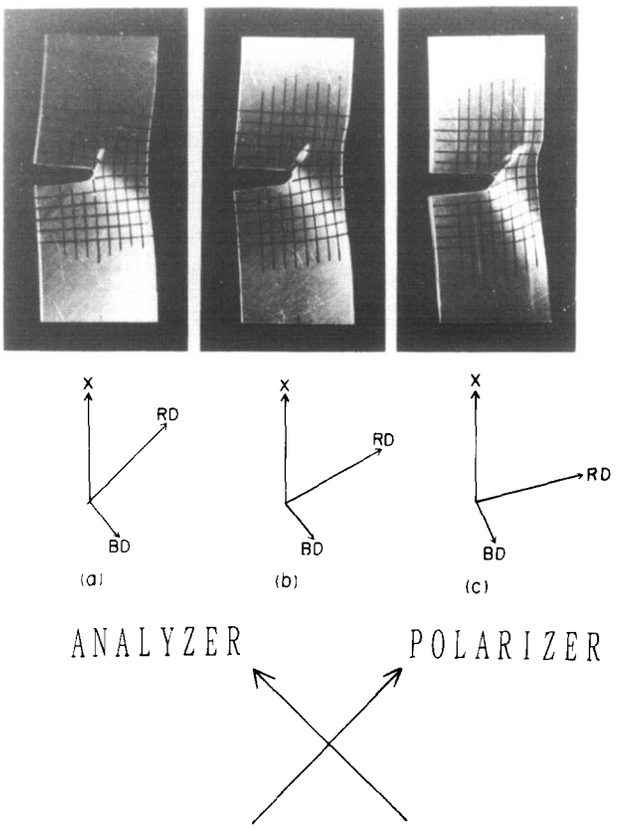

Figure 16 Kink bands of sample B with off-axis angles of (a) 45° (b) 60° and (c) 75°. X, stretch direction; RD, roll direction; BD, kink band direction. Displacements are all 1.5 mm

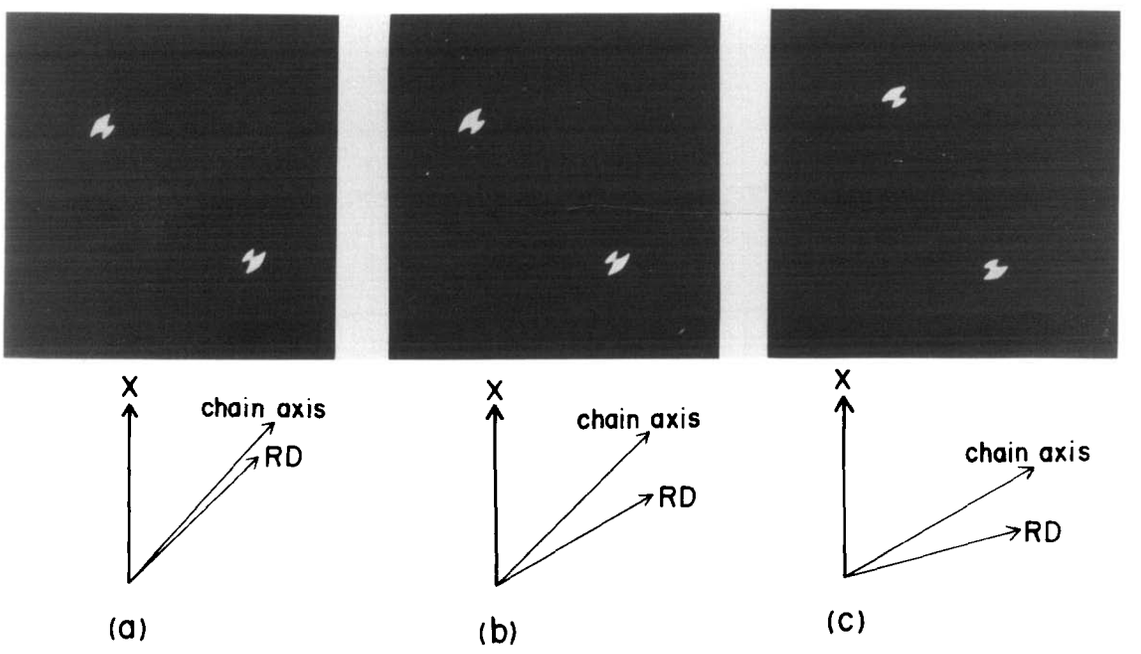

Figure 17 WAXD of the plastically deformed part inside the kink band. (a), (b) and (c) correspond to *Figure 16*

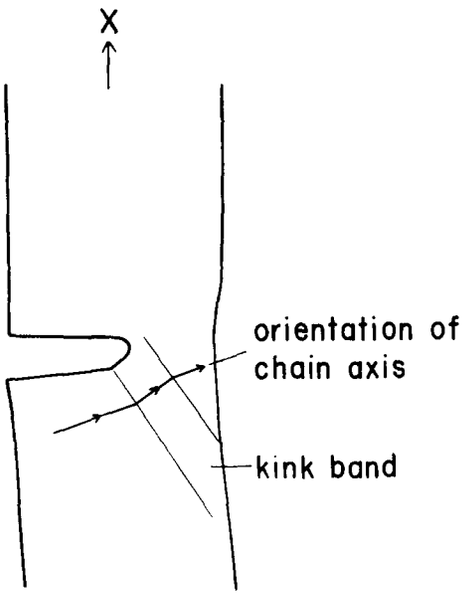

Figure 18 Relation of the sample coordinate with the chain axis and kink band of sample B with off-axis angle of 75°

molecular chains were oriented in the roll direction (RD). During stretching, molecular chains inside the kink band were reoriented toward the stretch direction so that the chain axes were not consistent with the RD. Such reorientation was due to kinking of the molecular chain by shear stress and stretch stress in the test direction. Consequently, the orientation of molecular chains under the crack plane was as shown in *Figure 18*.

As the experiment was performed at room temperature, which is above the glass transition temperature of polyethylene, the material would mostly fracture due to partition of the well aligned molecular chains rather than breakage of the chains. Thus, even though sample B did show global plastic deformation which was not consistent with the roll direction at the crack tip, the crack would still propagate in the roll direction. Existence of a crack provides a predictable location for stress concentration. It is believed that the above stress analysis can be used to interpret what happens to uncracked anisotropic materials because plastic deformation or fracture would commence from a weak position, which results from stress concentration.

CONCLUSION

Anisotropy of a material plays an important role in determining the stress distribution at the crack tip. Analysis of the mechanics of anisotropic cracked material leads to the following conclusions.

From application of the theory of plasticity and FEM, the stress distributions around the crack tip of anisotropic materials can be simulated using mechanical parameters from uncracked samples. The stress distributions depended on the chain axis directions. For a highly anisotropic material, σ_{xx} showed a maximum in the direction coincident with the chain axis. For material of less anisotropy, this trend was less defined. The shear stress τ_{xy}, which is small when compared with σ_{xx}, showed strong dependence on the off-axis angle for both samples A and B. At low off-axis angle, the shear stress above the crack plane was positive and larger in magnitude than the negative shear stress below the crack plane. As the off-axis angle increased, the shear stress below the crack plane became more intense. For the isotropic case, the shear stress is perfectly symmetrical with respect to the crack plane. In the case of an anisotropic material, the shear stress distribution was determined by the alignment of the chain axis.

The overall combination of the stress components was represented by the equivalent stress σ_e. For high anisotropic material, σ_e showed a maximum coincident with the chain axis at low off-axis angles. For low anisotropic material, a similar trend could be observed but not so clearly. The high modulus in the direction perpendicular to the roll direction of the low anisotropic material consequently increased the strength potential in the direction perpendicular to the chain axis of cracked sample. As the chain axis was aligned towards the crack plane, this effect began to dominate the plastic deformation. This resulted in the formation of the global plastic kink band deformation under the crack plane. Inside the kink band, the molecular chain was reoriented toward the stretch direction due to the combined effect of σ_{xx} and τ_{xy}. However, despite the plastic deformation, the crack always propagated in the chain axis direction.

REFERENCES

1 Young, R. J., Bowden, P. B., Ritchie, J. M. and Rider, J. G. *J. Mater. Sci.* 1973, **8**, 23
2 Robertson, R. and Joynson, C. W. *J. Appl. Phys.* 1966, **37**, 3969
3 Robertson, R. *J. Polym. Sci., A-2* 1969, **7**, 1315
4 Robertson, R. *J. Polym. Sci., A-2* 1969, **9**, 1255
5 Tajima, Y. *Jap. J. Appl. Phys.* 1973, **12**, 40
6 Brown, N. and Ward, I. M. *Phil. Mag.* 1968, **17**, 961
7 Brown, N., Duckett, R. A. and Ward, I. M. *Phil. Mag.* 1968, **18**, 483
8 Duckett, R. A., Goswami, B. C. and Ward, I. M. *J. Polym. Sci., Polym. Phys. Edn* 1972, **10**, 2167
9 Rider, J. G. and Hargreaves, E. *J. Polym. Sci., A-2* 1969, **7**, 829
10 Parrish, M. and Brown, N. *J. Macromol. Sci.-Phys.* 1970, **B4**, 649
11 Wang, M.-D., Nakanishi, E. and Hibi, S. *Polymer* 1993, **34**, 2783
12 Wang, M.-D., Nakanishi, E. and Hibi, S. *Polymer* 1993, **34**, 2792
13 Tsai, S. and Wu, E. *J. Compos. Mater.* 1971, **5**, 58
14 Yamada, Y., Yoshimura, N. and Sakurai, T. *Int. J. Mech. Sci.* 1968, **10**, 343
15 Hibi, S., Maeda, H. S., Hayashi, T. and Yamana, T. *Kobunshi Ronbunshu* 1983, **40** (7), 457